International Journal of Mechanical Sciences 106 (2016) 117–127

Contents lists available at ScienceDirect

International Journal of Mechanical Sciences

journal homepage: www.elsevier.com/locate/ijmecsci

Spherical indentation method to evaluate material properties of high-strength materials

Minsoo Kim [a], Karuppasamy Pandian Marimuthu [a], Jin Haeng Lee [b], Hyungyil Lee [a,*]

[a] Department of Mechanical Engineering, Sogang University, Seoul 04107, Republic of Korea
[b] Research Reactor Mechanical Structure Design Division, Korea Atomic Energy Research Institute, Daejeon 34057, Republic of Korea

ARTICLE INFO

Article history:
Received 7 July 2015
Received in revised form
2 December 2015
Accepted 10 December 2015
Available online 17 December 2015

Keywords:
Spherical indentation
Finite element analysis
High-strength
Material properties
Stress–strain curve

ABSTRACT

The spherical indentation method of Lee et al. (2005, 2010) [8,10] is extended for property evaluation of high-strength materials. By considering the finite deformation of elastic indenter due to high-strength of the indented material, regression functions are generated to map the indentation load–depth curve into the stress–strain curve. A property evaluation program is then written to produce material properties by using the indentation load–depth data from the loading/unloading process. Finally, the nano-indention tests with a spherical indenter are carried on Germanium Ge (100) and Silicon Si (100) to verify the proposed method using the experimental load–depth curves.

1. Introduction

High-strength materials have wide applications to cutting tools, surface coatings, components for high temperature, light weight automotive structures. In the applications, it is essential to understand the deformation behavior of material to applied load, i.e. stress–strain relationship. Young's modulus E, yield strength σ_o, strain hardening coefficient n are often used to describe the stress–strain relation.

For general metallic and brittle materials, numerous studies and techniques are available in the literature to evaluate these material properties from experimental test data [1]. Tensile/compression tests are traditionally used to determine the properties of metallic materials; however, standard specimens including elaborate machining jobs are needed to accomplish these tests [1]. On the other hand, a non-destructive and localized indentation method can be used with micro-size and non-standard specimens to evaluate constitutive properties, hardness, fracture toughness, residual stress and creep properties. In contrast to its rather simple testing process, extracting properties from the indentation test is far from being easy due to the non-uniform deformation beneath the indenter.

Numerous studies are thus carried out to reveal the characteristics of indention tests [2–10]. In indentation test, required properties are reversely extracted from the indentation load–depth curves (and imprint size) generally by using mapping functions. Sharp indentation produces phase transformation and micro-cracking even at relatively small loads. The indenter sharpness has significant effect on the mechanisms and it is hard to achieve the exact tip-sharpness during the manufacturing process. All these factors make the problem quite complex to be expressed analytically. In spherical indentations, phase transformation and micro-cracking can be avoided.

Tabor [11] proposed an idea to relate the mechanical properties with indentation load and depth. Afterwards, spherical indentation techniques are mainly studied to extract mechanical properties from experimental and numerical data [12–21]. Via extensive finite element (FE) analyses, Lee et al. [8,10] generated the functions mapping the indentation load–depth curve into the true stress–strain curve. They then contrived numerical algorithms which give the material properties of metallic materials from the load–depth data of spherical indentation test. Their reverse approaches provide the properties of general metallic material with high accuracy. However, the used material property ranges $\sigma_o < 1$ GPa keep the method from applying to high-strength materials.

For high-strength materials, relatively higher load is necessary to indent the specimen up to the same indentation depth. Consequently, the elastic indenter experiences finite deformation, the consideration of which is essential in the indentation of high-strength materials. The above studies [8–21] are mostly based on rigid or elastic indenter with negligible indenter deformation; therefore, one cannot directly apply these spherical indentation

* Corresponding author. Tel.: +82 2 705 8636; fax: +82 2 712 0799.
E-mail address: hylee@sogang.ac.kr (H. Lee).

http://dx.doi.org/10.1016/j.ijmecsci.2015.12.008
0020-7403/

studies for property evaluation of high-strength materials. However, Albayrak et al. [22] evaluated the E and σ_o of transparent Yttria (high-strength material) based on the spherical-tip assumption, while they considered the indenter deformation via effective modulus. Based on spherical-tip approximation, the solution with an irregular indenter tip shape can rather give reasonable elastic load-displacement relationship, but significantly arbitrary stress distribution and contact area beneath the indenter.

A reliable indentation method for evaluation of material properties of high-strength materials can be especially useful, when the cracking of specimen is hard to control during specimen preparation and testing due to the brittleness of material. For example in the tensile test, brittle materials are broken even at very small strain. Despite this compelling usefulness of indentation test, studies on the indentation methods for property evaluation of high-strength materials are limited in the literature.

In this study, by extending the method of Lee et al. [10], a technique is developed to evaluate the properties of high-strength materials from spherical indentation. Considering finite deformation of elastic indenter, we generate enhanced mapping functions. The range of yield strain is divided into three sections based on the regression characteristics; an independent program is generated for each section, and then 3 independent programs are integrated into a single property evaluation program. By applying the program to the spherical indentation test, material properties are obtained from a single indentation load–depth curve. Finally, the nano-indention tests with spherical indenters are carried on Germanium Ge (100) and Silicon Si (100) to verify the proposed method by using the experimental load–depth curves.

2. Finite element model for spherical indentation

The axisymmetric FE model (Fig. 1) for the spherical indentation simulation is formed, and the commercial FE software Abaqus/standard (ver. 6.12) [23] is used for the FE analysis. Considering axisymmetry of both geometry and loading, 4-node axisymmetric elements (CAX4) are used to model the indenter and specimen. To capture the large deformation and steep stress gradient, the sub-indenter region is refined with relatively small elements. To merge the small elements with large elements, the trapezoidal elements are used near the contact region, where the constrained mid-nodes in multi-point constrain (MPC) [23] tends to give discrete stress and strain values [8]. Therefore, MPC is used only in the region far from the contact region. The axisymmetric FE model consists about 16,700 nodes and 16,000 elements. For the spherical indenter with diameter $D=1\,\mu m$, the diamond material properties (Young's modulus $E_I=1000$ GPa, Poisson's ratio $\nu_I=0.07$) are assigned, while the friction coefficient $f=0.1$ is considered in the contact between indenter and the specimen [11,24].

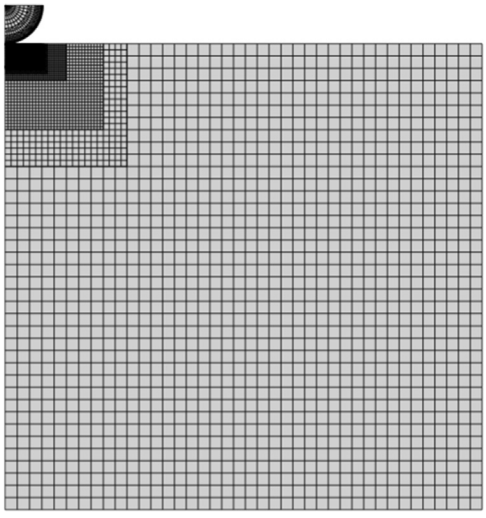

Fig. 1. FE model for $h_{max}/D=20\%$ indentation analyses.

A point at $l/D=0.3$, $2r/d=0.8$, where the strain gradient is relatively small [10], is selected as a data acquisition point to avoid the frictional effect on the effective stress σ and plastic strain ε_p measurements. Here l and r denote the vertical and radial distance, respectively, from the center of the contact, and d denotes the *actual* contact diameter. Note that the use of data acquisition point is only practical in FE simulations and cannot be applied in the experiments. The non-linear geometry change (NLGEOM) FE analyses are performed for the isotropic elasto-plastic materials, which obey J_2 incremental plastic theory.

In a shallow spherical indentation, the indenter deformation is insignificant due to relatively small indentation load P at shallow indentation depth; there is no finite indenter deformation. When the maximum indentation depth is relatively small, materials with different properties can yield almost identical load–depth curves, which result in significant errors of evaluated material properties [8,10]. It can be solved by increasing the indentation depth. In this study, 20% of indenter diameter is thus selected as a maximum indentation depth ($h_{max}/D=20\%$) as that of Lee et al. [10].

2.1. Material model for FE analysis

Eq. (1) is used here to express the stress–strain relationship with Hollomon's piecewise power law hardening material model [25].

$$\frac{\epsilon_t}{\epsilon_o}=\begin{cases}\frac{\sigma}{\sigma_o} & \text{for } \sigma\le\sigma_o\\ \left(\frac{\sigma}{\sigma_o}\right)^n & \text{for } \sigma\ge\sigma_o \;;\; 1<n\le\infty\end{cases} \tag{1}$$

Here σ_o, ε_o $(=\sigma_o/E)$, ε_t are the yield strength, yield strain and total strain, respectively. ε_t $(=\varepsilon_e+\varepsilon_p)$ is equal to the sum of elastic and plastic strains and n is the strain-hardening exponent. The material is assumed as perfectly elastic for $n=1$ and elastic-perfectly plastic for $n=\infty$. For $1<n<\infty$, the material shows the hardening behavior. Differently from the Ramberg–Osgood material model in other studies, the power-law functions of Eq. (1) has clear distinction between elastic and plastic regions at ε_o.

2.2. Enhanced evaluation of indentation contact diameter

Fig. 2 compares the diamond indenter deformation with rigid indenter, when $E=300$ GPa, $\varepsilon_o=0.1$, $n=3$ are used as the specimen material properties. The diamond indenter deviates from the spherical shape due to large deformation. In FE study, d is calculated from the nodal coordinates of the last nodes in contact,

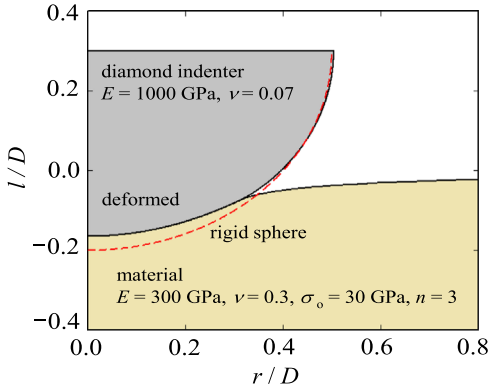

Fig. 2. Deformed shape of diamond indenter at loaded state.

which can be obtained by checking the contact status of nodes. If we assume that the contact diameter d is up to the last node with non-zero contact pressure, then the maximum error in d calculation is half of the element size e. Considering this, we evaluate d by taking the intersection (-✦-) of two lines that pass through the last two nodes in contact and first two nodes not in contact, respectively (Fig. 3) following the idea of Hay and Crawford [26]. Fig. 4 compares the calculated d values from intersection method (solid line) with those calculated from the last node in contact (open circle). The difference in d values from two methods is less than 0.2%. To detect the deformation carefully in the FE analyses, 0.0625% of the indenter diameter is used as a minimum element size at the surface.

3. Property evaluation techniques

3.1. Evaluation of Young's modulus from unloading part of load–depth curve

Young's modulus E is closely related to initial slope S in the unloading load–depth curve and the actual contact area [9,20,27]. Sneddon [27] and Pharr et al. [28] proposed an equation to predict E from S based on the assumption of an axisymmetric indenter penetrating the specimen. The effective modulus was introduced to include the deformation of the indenter. During the indentation, the materials exhibit pile-up/sink-in, which significantly depend on material properties and indentation depth. To consider the effect of pile-up/sink-in on actual contact area measurements, Lee et al. [8] introduced a correction factor κ into Young's modulus formula for the elastic–plastic materials as

$$E=\frac{1-\nu^2}{d_{\max}/(\kappa S)-(1-\nu_I^2)/E_I} \tag{2}$$

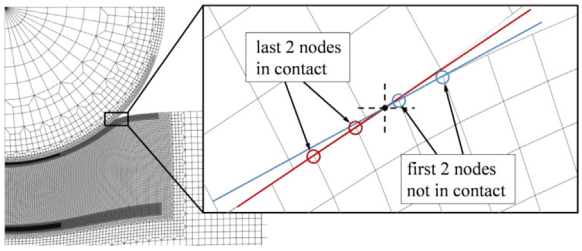

Fig. 3. Evaluation of d by taking the intersection (-✦-) of two lines that are passing through the last two nodes in contact and first two nodes not in contact, respectively [26].

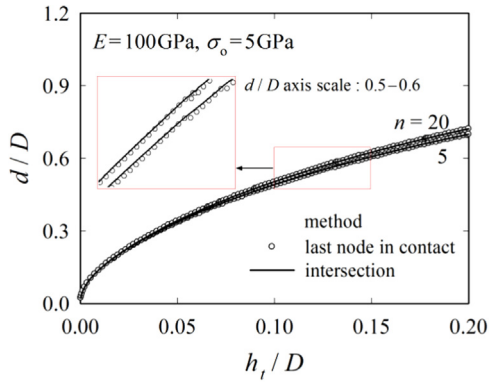

Fig. 4. d/D vs. h_t/D for various values of n; open symbol from last contact node and solid line from intersection point.

where the maximum contact diameter $d_{\max}$ is measured at $h_{\max}$ by considering the effect of pile-up/sink-in. E and E_I are the Young's modulus, ν and ν_I are the Poisson's ratios of the specimen and indenter, respectively. The regression range ($r_s<0.1$) used for linear regression of S is defined as

$$r_s \equiv (P_{\max}-P)/P_{\max} \tag{3}$$

$P_{\max}$ is the maximum load at $h_{\max}$. S decreases with increasing r_s, and it converges for $r_s<0.1$ [8].

In the indention test and FE analysis, pile-up/sink-in phenomena near the contact edge make it difficult to accurately measure or predict the actual contact diameter d (or contact area). With the rigid spherical indenter, the actual contact diameter can be obtained from the shape of spherical geometry even with the pile-up/sink-in phenomena as follows

$$d=2\sqrt{hD-h^2}=2\sqrt{c^2h_tD-(c^2h_t)^2} \tag{4}$$

where h is the real indentation depth, when pile-up/sink-in phenomenon occurs during the indentation. h_t is the indentation depth measured from the reference surface. Hill et al. [29] defined c^2 as the ratio of h and h_t ($c^2\equiv h/h_t$). As it is difficult to measure d, Lee et al. [10] expressed c^2 as a function of indentation depth h_t and the material properties based on the FE analyses in the form of Eq. (5). The calculated c^2 values from Eq. (5) are then used in Eq. (4) to obtain the actual contact diameter d.

$$c^2=f_0^d(\varepsilon_o,n,E/E_I)+f_1^d(\varepsilon_o,n,E/E_I)\ln(h_t/D) \tag{5}$$

Lee et al. [10] used c^2 of Eq. (5) to calculate d in Eq. (4), which is valid for a rigid indenter or an elastic indenter with negligible deformation. By performing indentation FE analyses with general metallic materials (σ_o=100–3000 MPa), Lee et al. [10] wrote a property evaluation program with Eqs. (3) and (4), while they considered the elastic spherical indenter with negligible indenter deformation. For high-strength materials (σ_o=1–30 GPa), their property evaluation program with Eqs. (3) and (4) may result in large error due to finite indenter deformation. Therefore, we consider the finite indenter deformation for high-strength materials in the FE analyses to improve the functions for d evaluation. For E=100 GPa, σ_o=5 GPa, ε_o=0.05, n=3, 5, and 20, Fig. 5 shows the variation of d against indentation depth h_t. As Eq. (2) requires $d_{\max}$ only, not the variation of d with h_t, therefore only upper 25% of data is used for linear regression as illustrated in Fig. 5. The regression of (d/D) is given as

$$\begin{aligned}
&(d/D)=f_0^d(\varepsilon_o,n,E/E_I)+f_1^d(\varepsilon_o,n,E/E_I)\ln(h_t/D)\\
&f_i^d(\varepsilon_o,n,E/E_I)=\alpha_{ij}^d(\varepsilon_o,E/E_I)n^{-j}\quad;\quad i=0,1,\quad j=0,1\\
&\alpha_{ij}^d(\varepsilon_o,E/E_I)=\beta_{ijk}^d(E/E_I)\varepsilon_o^k\quad;\quad k=0,\ 1,\ 2,\ 3\\
&\beta_{ijk}^d(E/E_I)=\gamma_{ijkl}^d\quad;\quad l=0,1,\ 2
\end{aligned} \tag{6}$$

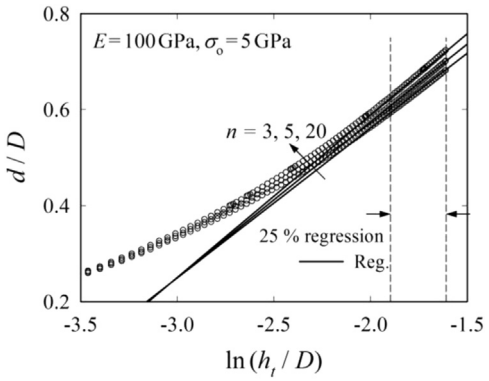

Fig. 5. Regression curves of d/D vs. $\ln(h_t/D)$ for various values of n.

With this proposed method for high-strength materials, one can calculate d_{max} directly from Eq. (6) at corresponding h_{max}. Then, Eq. (2) can be recast as

$$\kappa = \frac{d_{max}}{S}\left(\frac{1-\nu^2}{E}+\frac{1-\nu_I^2}{E_I}\right)^{-1} \tag{7}$$

κ is calculated by substituting the initial slope S (regression range: $r_s < 0.1$) of unloading load–depth curve into Eq. (7). The regression of κ is given as

$$\begin{aligned}
&\kappa = f_i^{\kappa}(\varepsilon_o, n, E/E_I) = \alpha_j^{\kappa}(\varepsilon_o, E/E_I)n^{-j} \quad ; \quad j = 0,\ 1,\ 2\\
&\alpha_j^{\kappa}(\varepsilon_o, E/E_I) = \beta_{jk}^{\kappa}(E/E_I)\varepsilon_o^{k} \quad ; \quad k = 0,\ 1,\ 2,\ 3,\ 4\\
&\beta_{jk}^{\kappa}(E/E_I) = \gamma_{jkl}^{\kappa} \quad ; \quad l = 0,\ 1,\ 2
\end{aligned} \tag{8}$$

Table 1 lists various material property values used for finite element analyses and accompanying regression.

3.2. Evaluation of yield strength and strain hardening coefficients

The only information from the indentation test is the load–depth curve; it should be converted into the stress–strain curve, which is expressed in terms of E, σ_o and ε_o in the power-law material model.

When $\sigma \geq \sigma_o$, the Eq. (1) can be written as follows

$$\sigma = \sigma_o\left(\varepsilon_t/\varepsilon_o\right)^{1/n} = K\varepsilon_t^{1/n} \tag{9}$$

where the strength coefficient K and strain hardening coefficient n are obtained by regressing the stress–strain data calculated from indentation load–depth curve. At yield point, Eq. (9) becomes

$$\sigma_o = K\varepsilon_o^{1/n} \tag{10}$$

The elastic stress–strain relation at yield point is given as

$$\sigma_o = E\varepsilon_o \tag{11}$$

By combining Eq. (10) with Eq. (11), the yield strength is given as

$$\sigma_o = \left(K^n/E\right)^{\frac{1}{n-1}} = E(K/E)^{\frac{n}{n-1}} \tag{12}$$

By substituting n and K values [obtained from the regression of stress–strain data with Eq. (9)], the yield strength σ_o can be obtained from Eq. (12). Based on ε_p and σ values at the data acquisition point (l/D=0.3, $2r/d$=0.8) in the FE analyses, we express ε_p and σ as functions of h_t/D and material properties as follows

$$\begin{aligned}
&\varepsilon_p = f_i^{\varepsilon}(\varepsilon_o, n, E/E_I)\left(\frac{h_t}{D}\right)^i\\
&f_i^{\varepsilon}(\varepsilon_o, n, E/E_I) = \alpha_{ij}^{\varepsilon}(\varepsilon_o, E/E_I)n^{-j} \quad ; \quad i = 0,1,2,3, \quad j = 0,1,2,3,4\\
&\alpha_{ij}^{\varepsilon}(\varepsilon_o, E/E_I) = \beta_{ijk}^{\varepsilon}(E/E_I)\varepsilon_o^{k} \quad ; \quad k = 0,1,2\\
&\beta_{ijk}^{\varepsilon}(E/E_I) = \gamma_{ijkl}^{\varepsilon} \quad ; \quad l = 0,1,2
\end{aligned} \tag{13}$$

$$\begin{aligned}
&\psi = \frac{P}{D^2\sigma} = f_i^{\psi}(\varepsilon_o, n, E/E_I)\left(\frac{h_t}{D}\right)^i\\
&f_i^{\psi}(\varepsilon_o, n, E/E_I) = \alpha_{ij}^{\psi}(\varepsilon_o, E/E_I)n^{-j} \quad ; \quad i = 0,1,2,3, \quad j = 0,1,2,3,4
\end{aligned}$$

Table 1
Material properties for FE analyses.

Parameter	Values used for FEA
E	100, 200, 300 GPa
ν	0.3
ε_o	0.01–0.1
n	1.1, 1.5, 2, 2.5, 3, 4, 5, 7, 10, 13, 20, 50
f	0.1

$$\begin{aligned}
&\alpha_{ij}^{\psi}(\varepsilon_o, E/E_I) = \beta_{ijk}^{\psi}(E/E_I)\varepsilon_o^{k} \quad ; \quad k = 0,1,2\\
&\beta_{ijk}^{\psi}(E/E_I) = \gamma_{ijkl}^{\psi} \quad ; \quad l = 0,1,2
\end{aligned} \tag{14}$$

The effective stress is calculated from $\sigma \equiv P/(D^2\psi)$. Note that D is used to normalize the indentation variables of Eqs. (6), (13) and (14). On the other hand, d_{max} is used for normalized expression of κ in Eq. (7) to reduce the sensitivity of κ to the material properties. The four normalized indentation variables (d/D,ε_p,ψ,κ) with improved regression functions are used to generate property evaluation programs for high strength materials.

4. Property evaluation program for high-strength materials

4.1. Evaluation of material properties using proposed method

For ε_o (=0.01, 0.03, and 0.05), n (=5, and 50) and E=100 GPa, the variations of ε_p with h_t are measured at the data acquisition point (l/D=0.3, $2r/D$=0.8) as shown in Fig. 6(a)–(c). Note that the relationship between ε_p and h_t becomes linear as ε_o increases or n decreases. The stress variable ψ also shows the same trend. Variations of ε_p and ψ with h_t are thus regressed in the form of Eqs. (13) and (14) by dividing the range of ε_o into three sections. The sections for ε_o=0.01–0.03, 0.03–0.05 and 0.05–0.1 are regressed with 3, 2 and 1 degree of polynomial, respectively. Based on the three regression functions, we write three property evaluation programs A, B and C for each section.

The flow chart of the property evaluation programs is shown in Fig. 7. After the indentation to h_{max}=0.2D, the load–depth curve is given as input data to the property evaluation program. Initial value of S is calculated from the unloading load–depth curve. For the first iteration, we assume the initial values of E^i, ε_o^i , n^i.

Based on the given load–depth data and the assumed values of E^i, ε_o^i , n^i, the variation of d^i, ε_p^i, ψ^i are calculated from Eqs. (6), (13) and (14), and then ψ^i is converted into σ^i. By updating data values of ε_p^i and σ^i into Eq. (9), we convert the load–depth curve into the corresponding stress–strain curve, thus the values of K^{i+1} and n^{i+1} are computed from the regression of stress–strain data. E^{i+1} is then calculated by using Eqs. (2) and (7), where we use the initial slope S and d_{max}^i calculated from Eq. (6) for h_{max}. Finally, E^{i+1}, K^{i+1} and n^{i+1} are substituted into Eqs. (11) and (12) to calculate yield strength $\sigma_o^{i+1}$and yield strain ε_o^{i+1}, which are again used to update E^{i+1}. The calculated $\varepsilon_o^{i+1}$and n^{i+1} are compared with previous ε_o^i and n^i values to compute the relative change e

$$e = \mathrm{Max}\left(\frac{\varepsilon_o^{i+1}-\varepsilon_o^i}{\varepsilon_o^i}, \frac{n^{i+1}-n^i}{n^i}\right) \tag{15}$$

The above steps are repeated until the relative changes are converged within the tolerance. At the end, the material properties E, σ_o and n are achieved from the given indentation load–depth curve.

Using the property evaluation programs A, B and C, we calculate the yield strength σ_o as shown in Fig. 8 for ε_o=0.03 and 0.05, which are the boundary values for program A (ε_o=0.01–0.03) and B (0.03–0.05), program B and C (0.05–0.1), respectively. Although three programs use different polynomial degrees for regression, we get σ_o with an average error of 1% for the boundary values of ε_o=0.03 and 0.05. For E (=100, 200, and 300), n (=5, 7, 13, and 20) and ε_o (=0.01–0.1), computed values of $\varepsilon_o|_{computed}$ from the program C, which is valid for ε_o=0.05–0.1, are given as symbols in Fig. 9. If $\varepsilon_o < 0.05$, then always $\varepsilon_o|_{computed} < 0.05$. Similarly, the program B valid for ε_o=0.03–0.05 always gives $\varepsilon_o|_{computed} < 0.03$ if $\varepsilon_o < 0.03$. On this observation, by combining three programs A, B, C, an integrated property evaluation program for ε_o=0.01–0.1 is written with following condition that if the computed yield strain with program C is $\varepsilon_o|_{computed} < 0.05$, then the program B is used for

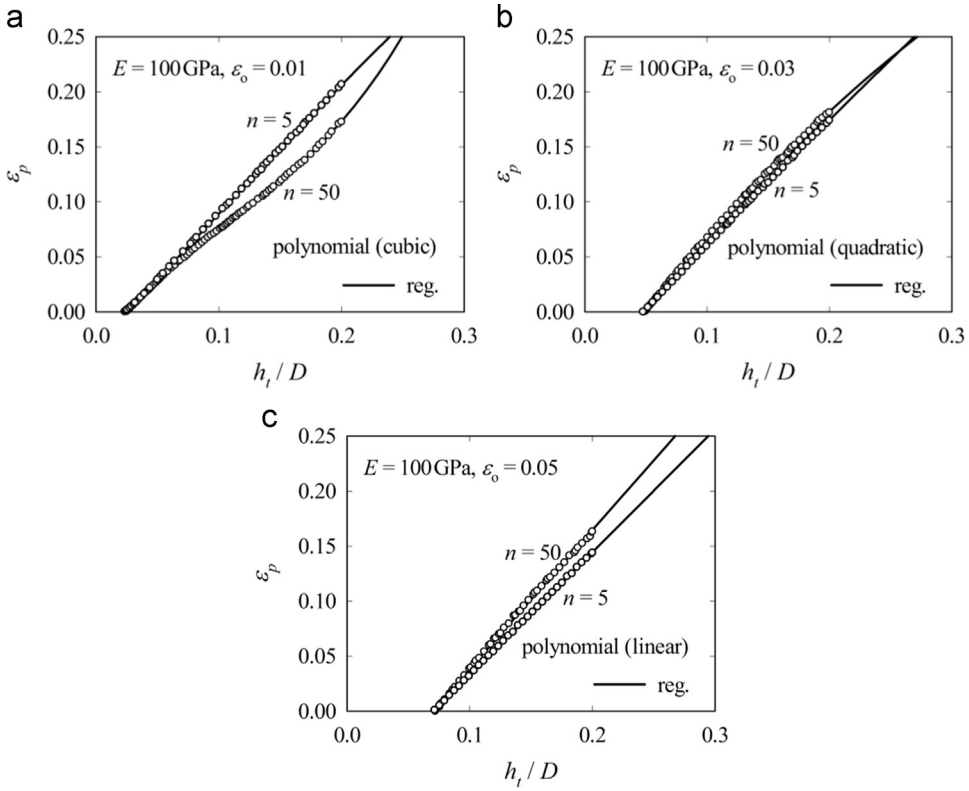

Fig. 6. Equivalent plastic strain vs. normalized indentation depth data.

property evaluation. Similarly, if $\varepsilon_{o|computed} < 0.03$, program A is used for property evaluation from the indentation load–depth curve.

For various properties of high-strength materials, Figs. 10–12 compare the stress–strain curves (symbols) computed from the property evaluation program to those given as input (solid line) for FE analyses. Table 2 lists the given and computed material properties with their relative deviations (errors). In the proposed method, E and σ_o are computed with an average error of 0.3% and 0.8%, respectively. We compute n with the average error of 6.4%.

In actual property evaluation, Hyun et al. [5] demonstrated that n is rather sensitive to the strain range for regression. It is thus necessary to select an appropriate regression range of material properties depending on the material.

5. Validation of property evaluation program by nanoindentation test

In the validation process, experimental load–depth curve is assigned as input data to the property evaluation program. The evaluated material properties from the program are then used as input data for the FE analysis to obtain FE load–depth curve. Finally, the property evaluation program is validated by comparing the experimental load–depth curve with that from FE analysis.

Nano Indenter-XP™ (Agilent Technologies) with diamond spherical indenter $D=1$ μm is used in the experimental indentation tests. In nanoindentation test, the creep [30] and thermal drift, which are difficult to distinguish, are very important sources of error in the material property evaluation such as E and hardness H. As the amount of creep depends on the loading rate and the holding period in the nanoindentation, the creep error on E measurements was reduced by holding the P_{max} for a holding period of 5 s or longer [31]. Although, significant creep effects at the onset of unloading i.e. a “nose” was observed in metals [32,33]. Therefore, Feng and Ngan [32] introduced a creep factor C to correct the creep error on E measurements. Also, they provided a condition to minimize the thermal drift during nanoindentation. Since experiments were conducted by placing the apparatus in an insulated enclosure at room temperature and with holding period of 10 s, we shall assume that the creep and thermal drift influences are not significant and can be neglected. The nanoindentation tests are carried out with silicon Si and germanium Ge crystal specimens with lattice plane (100). Values of Young's moduli for Si and Ge with lattice plane are shown in Table 3. The plastic anisotropy of materials remains as the future work.

For $h_{max}=200$ nm, Fig. 13 shows experimental load–depth curves from the indentation tests. During unloading, pop-out phenomenon is observed in the load–depth curves of Si (100) and Ge (100), which is consistent with the observation of Brady et al. [36]. The pop-out phenomenon occurs due to phase transformation, which is associated with volume and density changes of sub-indenter materials. There is a blunt turn between experimental loading and unloading curves due to very small creep deformation in the holding period. Therefore, we ignore very initial part of unloading data for accurate measurement of initial unloading slope S. The creep factor C [32] is calculated for Si (100) and Ge (100) as $C_{Si}=6.3\%$ and $C_{Ge}=7.9\%$, which are less than 10%; therefore the creep effects are small [32] and be neglected. With the measured S, the property evaluation program provides E values of Si (100) and Ge (100) close to literature values.

Table 4 lists the evaluated E, σ_o and n from experimental load–depth curve, and corresponding stress–strain curves are shown in Fig. 14. The solid lines regress the stress–strain data in the form of power-law function. For Si (100) and Ge (100), FE load–depth curves are obtained by using the evaluated material properties of Table 4. The load–depth curves from FE analyses are in good agreements with the experimental ones as shown in Fig. 15, where the three

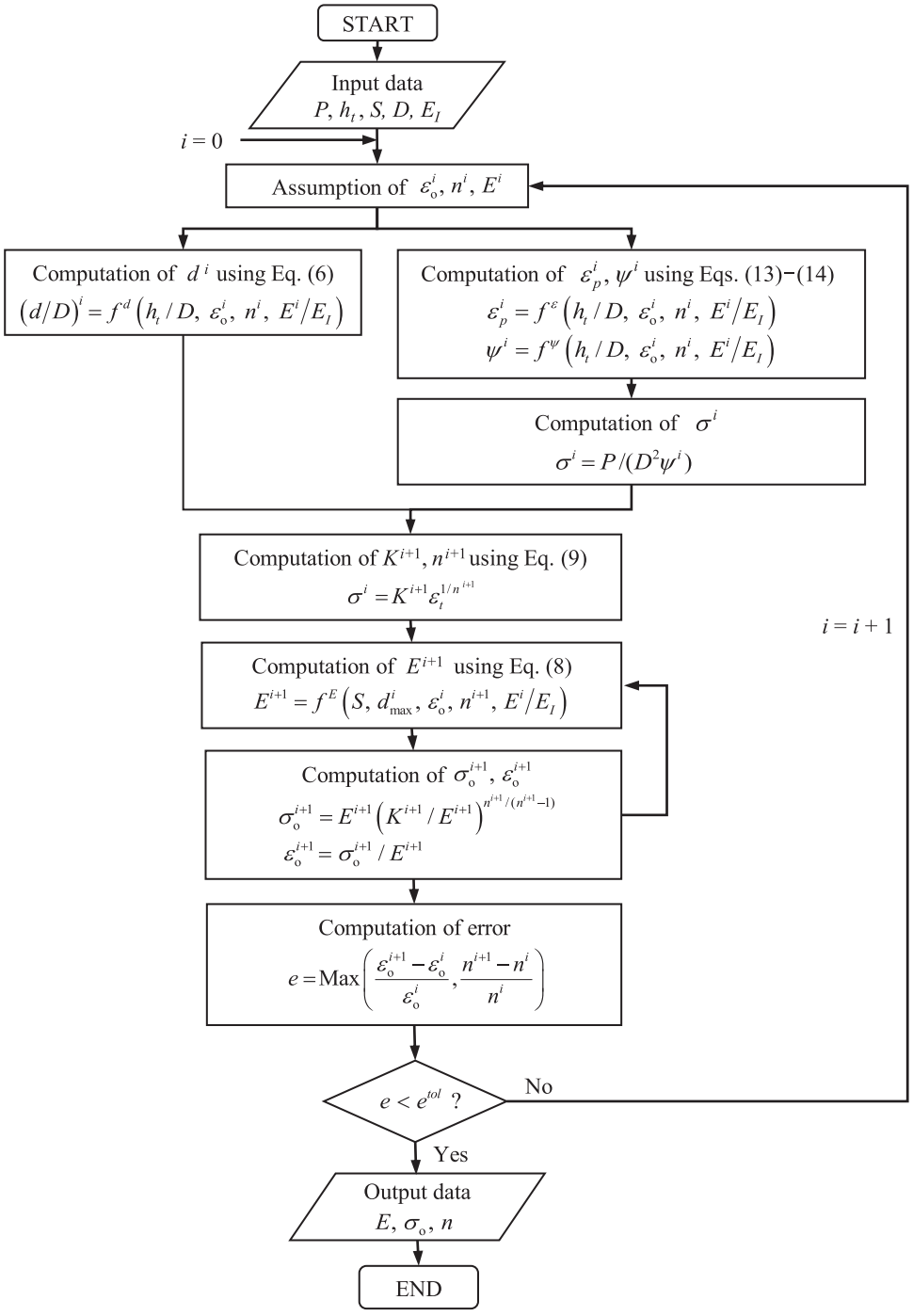

Fig. 7. Flow chart for determination of material properties.

test curves appear as a single curve. The creep deformation was included in the experimental load–depth curves, but not in the FE curves as it was not modeled, which causes some differences in the initial part of unloading curves between FEA and experiment. Fig. 15, in some sense, validates the algorithm in Fig. 7.

6. Summaries and conclusions

Based on FE analyses, the spherical indentation method of Lee et al. [8,10] was extended for property evaluation of high-strength materials. By considering the finite deformation of elastic indenter due to high-strength of the indented material, regression functions were newly generated to map the indentation load–depth curve into stress–strain curve. The property evaluation programs were then written to compute the material properties (E, σ_o, n) by using the indentation load–depth data measured from the loading/unloading process. Finally, the proposed property evaluation program was validated by using the experimental load–depth curves of Si (100) and Ge (100) from the nano-indention tests with a spherical indenter.

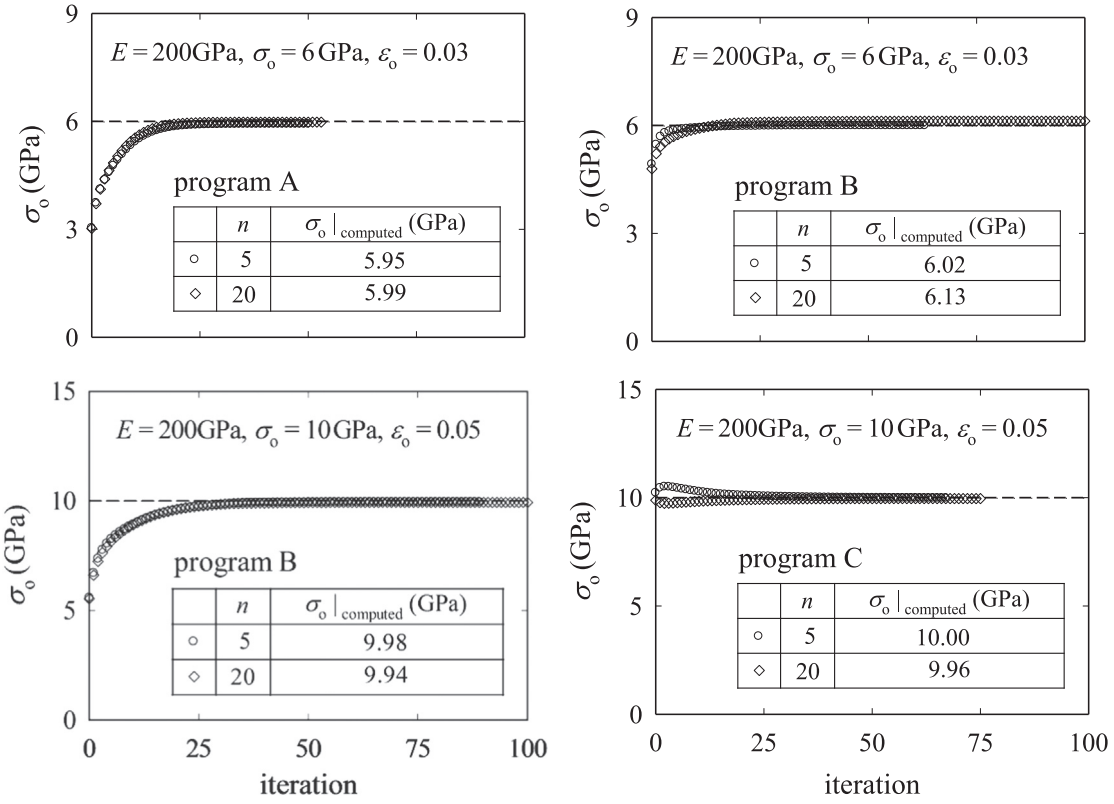

Fig. 8. $\sigma_o|_{computed}$ vs. iteration data; program A and B compute σ_o for ε_o=0.03, while program B and C compute σ_o for ε_o=0.05.

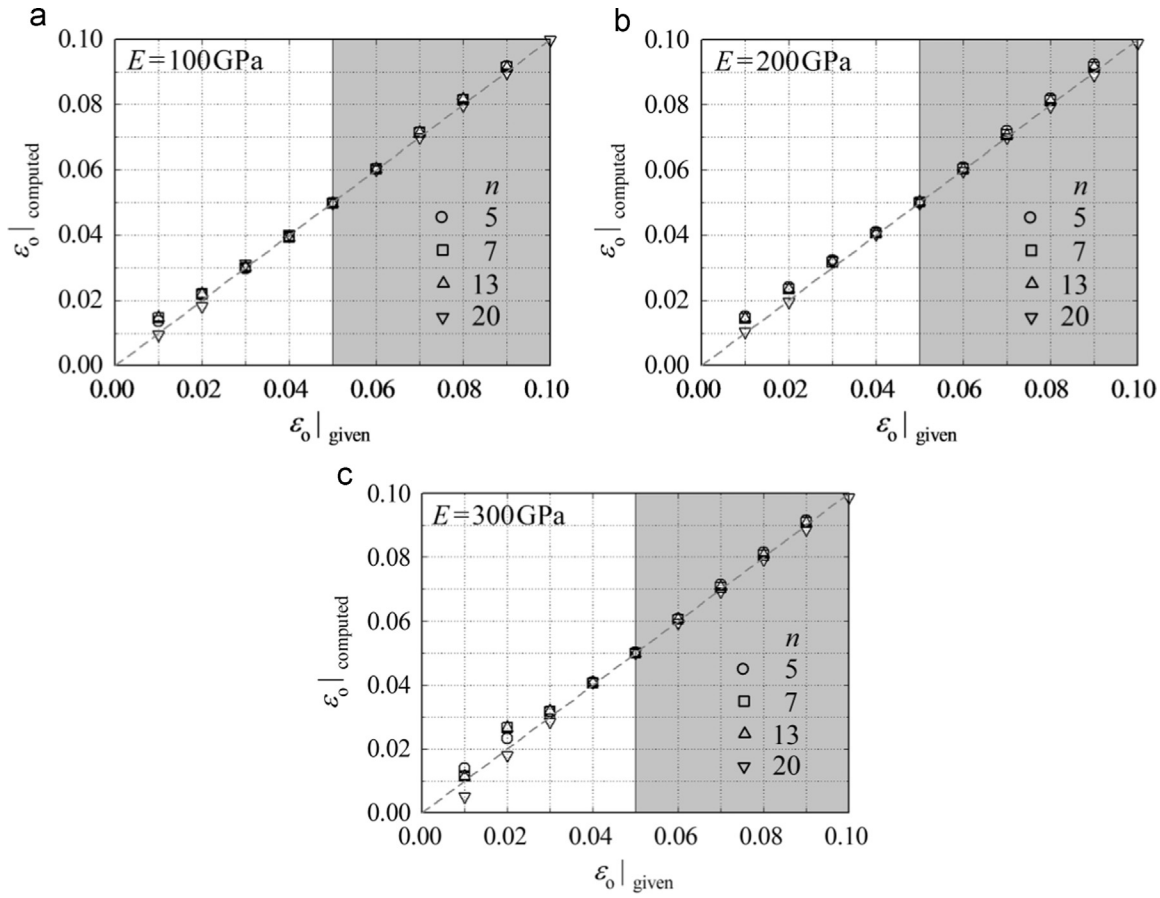

Fig. 9. Comparisons of $\varepsilon_o|_{computed}$ from program C with $\varepsilon_o|_{given}$ for (a) E=100, (b) E=200, and (c) E=300 GPa; program C is valid in the gray region only.

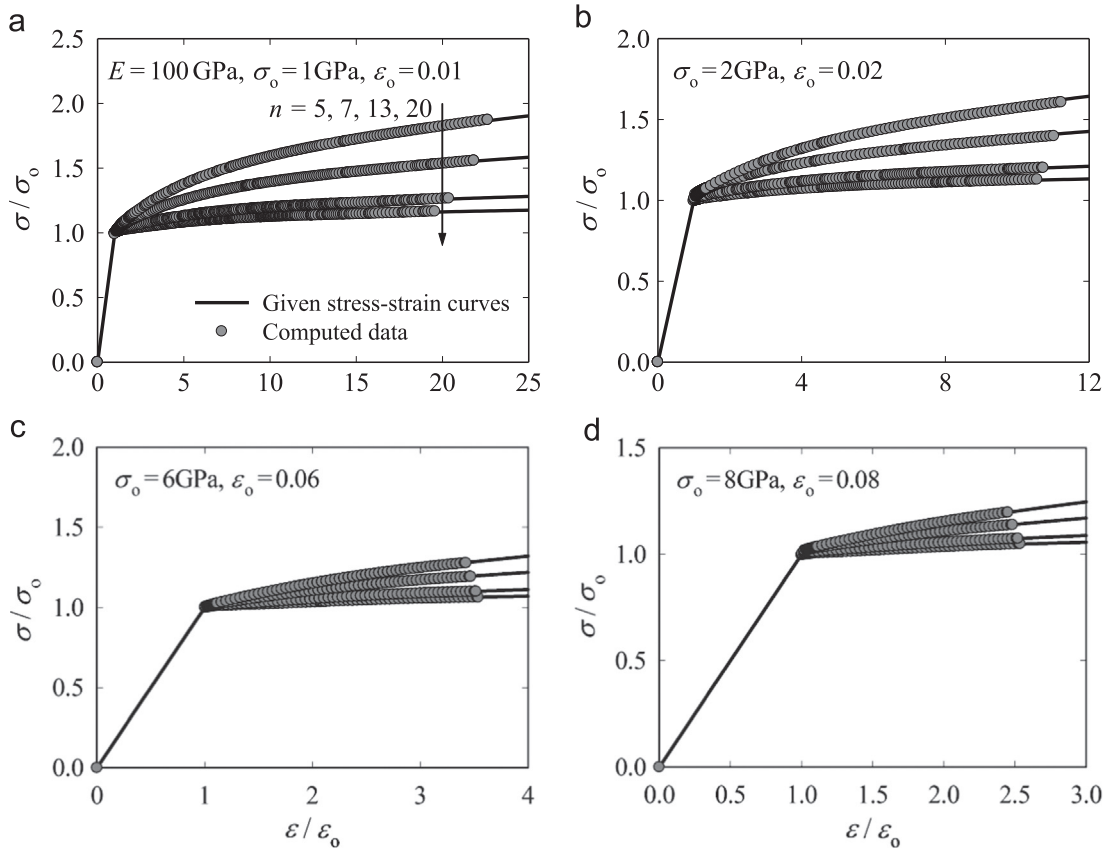

Fig. 10. Comparisons of computed stress–strain curves with those given for $E=100$ GPa [ε_o=(a) 0.01 (b) 0.02 (c) 0.06 and (d) 0.08].

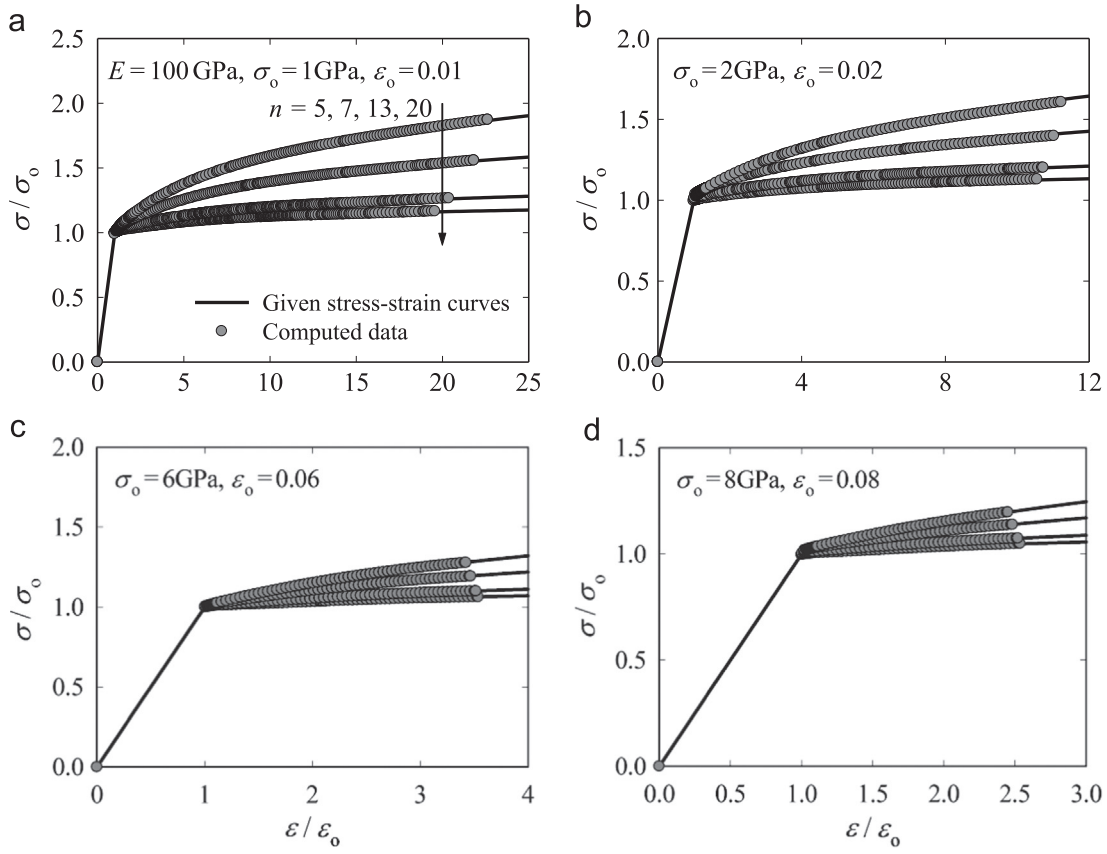

Fig. 11. Comparisons of computed stress–strain curves with those given for $E=200$ GPa [ε_o=(a) 0.01 and (b) 0.06].

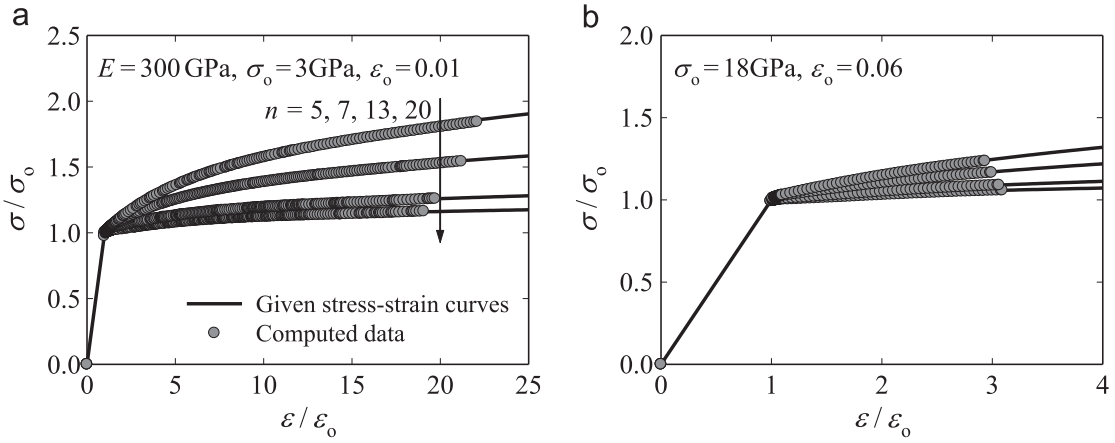

Fig. 12. Comparisons of computed stress–strain curves with those given for $E=300$ GPa [ε_o=(a) 0.01 and (b) 0.06].

Table 2
Comparison of computed material property values to those given.

σ_o/E (GPa)	n	Computed σ_o/E (GPa)	Error (%)	Computed n	Difference
1/100	5	0.99/100	1.0/0.0	4.8	−0.2
	7	1.00/100	0.0/0.0	6.9	−0.1
	13	1.00/100	0.0/0.0	12.6	−0.4
	20	1.00/100	0.0/0.0	18.9	−1.1
2/100	5	2.03/100	1.5/0.0	5.2	0.2
	7	2.07/100	3.5/0.0	7.9	0.9
	13	2.01/99	0.5/1.0	13.3	0.3
	20	1.99/100	0.5/0.0	18.7	−1.3
3/100	5	3.01/100	0.3/0.0	5.2	0.2
	7	3.02/100	0.7/0.0	7.2	0.2
	13	3.00/100	0.0/0.0	12.8	−0.2
	20	2.99/100	0.3/0.0	19.0	−1.0
4/100	5	4.04/100	1.0/0.0	5.1	0.1
	7	4.01/100	0.3/0.0	7.0	0.0
	13	4.00/100	0.0/0.0	12.9	−0.1
	20	4.03/100	0.8/0.0	21.7	1.7
5/100	5	5.03/100	0.6/0.0	5.0	0.0
	7	5.00/100	0.0/0.0	6.9	−0.1
	13	4.98/100	0.4/0.0	12.4	−0.6
	20	5.00/100	0.0/0.0	19.3	−0.7
6/100	5	6.03/100	0.5/0.0	5.0	0.0
	7	6.02/100	0.3/0.0	7.1	0.1
	13	6.00/100	0.0/0.0	12.9	−0.1
	20	6.01/100	0.2/0.0	20.8	0.8
8/100	5	8.15/100	1.9/0.0	5.5	0.5
	7	8.12/100	1.5/0.0	7.8	0.8
	13	8.02/100	0.3/0.0	13.4	0.4
	20	8.02/100	0.3/0.0	20.4	0.4
9/100	5	9.15/100	1.7/0.0	5.5	0.5
	7	9.13/100	1.4/0.0	7.9	0.9
	13	9.02/100	0.2/0.0	13.4	0.4
	20	8.96/100	0.4/0.0	17.9	−2.1
2/200	5	1.98/200	1.0/0.0	4.9	−0.1
	7	1.98/200	1.0/0.0	6.8	−0.2
	13	1.98/200	1.0/0.0	12.3	−0.7
	20	1.98/201	1.0/0.5	18.2	−1.8
4/200	5	3.98/199	0.5/0.5	5.0	0.0
	7	3.98/200	0.5/0.0	6.9	−0.1
	13	3.96/200	1.0/0.0	12.1	−0.9
	20	3.94/200	1.5/0.0	17.2	−2.8
6/200	5	6.02/200	0.3/0.0	4.9	−0.1
	7	6.03/200	0.5/0.0	7.0	0.0
	13	6.06/200	1.0/0.0	13.7	0.7
	20	6.13/200	2.2/0.0	26.3	6.3
8/200	5	8.03/200	0.4/0.0	4.9	−0.1
	7	8.01/200	0.2/0.0	6.8	−0.2
	13	7.97/200	0.4/0.0	12.0	−1.0
	20	7.96/200	0.5/0.0	17.6	−2.4
10/200	5	10.0/200	0.0/0.0	5.0	0.0
	7	10.0/200	0.0/0.0	7.0	0.0
	13	9.96/200	0.4/0.0	11.6	−1.4
	20	9.94/200	0.6/0.0	16.8	−3.2
12/200	5	12.1/200	0.8/0.0	5.2	0.2
	7	12.0/200	0.0/0.0	7.2	0.2
	13	12.0/200	0.0/0.0	13.0	0.0
	20	11.9/200	0.8/0.0	18.1	−1.9
16/200	5	16.3/200	1.9/0.0	5.6	0.6
	7	16.2/200	1.3/0.0	7.8	0.8
	13	16.0/200	0.0/0.0	12.7	−0.3
	20	15.9/200	0.6/0.2	17.3	−2.7
18/200	5	18.4/200	2.2/0.0	5.8	0.8
	7	18.3/200	1.7/0.0	8.0	1.0
	13	18.0/200	0.0/0.0	12.5	−0.5
	20	17.8/200	1.1/0.0	15.5	−4.5
3/300	5	2.93/300	2.3/0.0	4.8	−0.2
	7	3.00/299	0.0/0.3	7.0	0.0
	13	3.02/299	0.7/0.3	13.2	0.2
	20	2.98/301	0.7/0.3	18.4	−1.6
6/300	5	6.05/298	0.8/0.7	5.4	0.4
	7	6.13/298	2.2/0.7	7.7	0.7
	13	6.12/299	2.0/0.3	14.9	1.9
	20	5.95/301	0.8/0.3	18.2	−1.8
9/300	5	8.92/301	0.9/0.3	4.7	−0.3
	7	8.95/301	0.6/0.3	6.6	−0.4
	13	9.05/300	0.6/0.0	13.1	0.1
	20	8.97/300	0.3/0.0	18.0	−2.0
12/300	5	12.0/301	0.0/0.3	4.7	−0.3
	7	12.0/300	0.0/0.0	6.7	−0.3
	13	12.0/300	0.0/0.0	12.0	−1.0
	20	12.0/301	0.0/0.3	18.3	−1.7
15/300	5	15.0/300	0.0/0.0	5.1	0.1
	7	15.0/300	0.0/0.0	7.0	0.0
	13	15.0/300	0.0/0.0	12.8	−0.2
	20	15.0/300	0.0/0.0	20.5	0.5
18/300	5	18.2/300	1.1/0.0	5.3	0.3
	7	18.2/300	1.1/0.0	7.5	0.5
	13	17.9/300	0.6/0.0	12.3	−0.7
	20	18.0/300	0.0/0.0	17.9	−2.1
24/300	5	24.4/300	1.7/0.0	5.5	0.5
	7	24.2/300	0.8/0.0	7.6	0.6
	13	24.0/300	0.0/0.0	13.0	0.0
	20	23.8/300	0.8/0.0	16.7	−3.3
27/300	5	27.5/300	1.9/0.0	5.7	0.7
	7	27.2/300	0.7/0.0	7.6	0.6
	13	26.8/300	0.7/0.0	11.9	−1.1
	20	26.6/300	1.5/0.0	15.0	−5.0

Table 2 (*continued*)

Table 3
Young's moduli of Si and Ge with lattice plane.

lattice plane	E (GPa)		Reference
	Si	Ge	
(100)	130/129*	104	Wortman and Evans [34]/
(110)	169/168*	138	Callister and Rethwisch [35]*
(111)	188/187*	155	

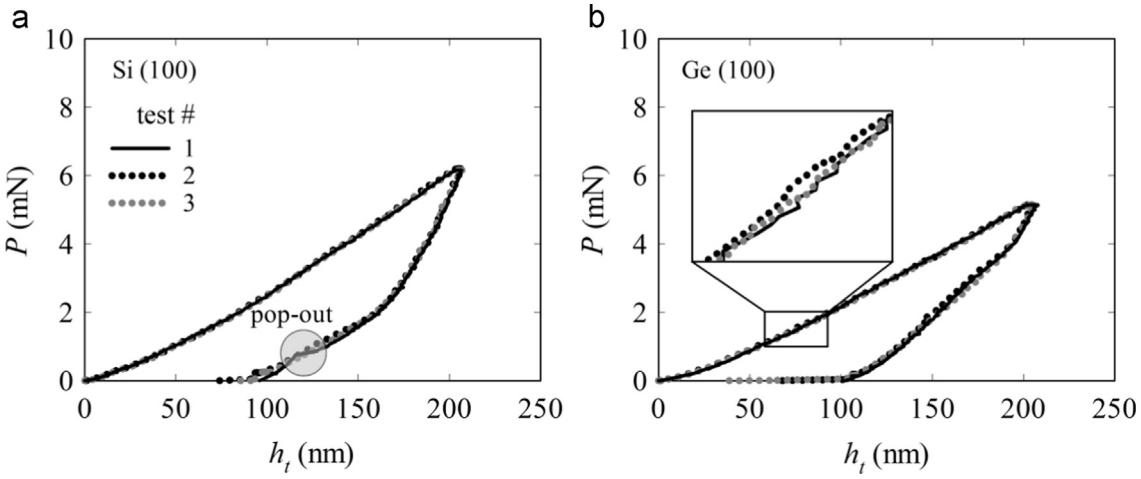

Fig. 13. Load–depth curves obtained from nano-indentation test for (a) Si (100) and (b) Ge (100).

Table 4
Material properties from spherical nano-indentation tests.

Material	Test #	E (GPa)	σ_o (GPa)	n
Si (100)	1	128	2.7	2.9
	2	132	2.5	2.9
	3	127	2.8	3.0
	Avg.	129.0	2.66	2.90
Ge (100)	1	101	3.1	3.8
	2	109	3.0	4.3
	3	109	3.0	4.3
	Avg.	106.3	3.04	4.12

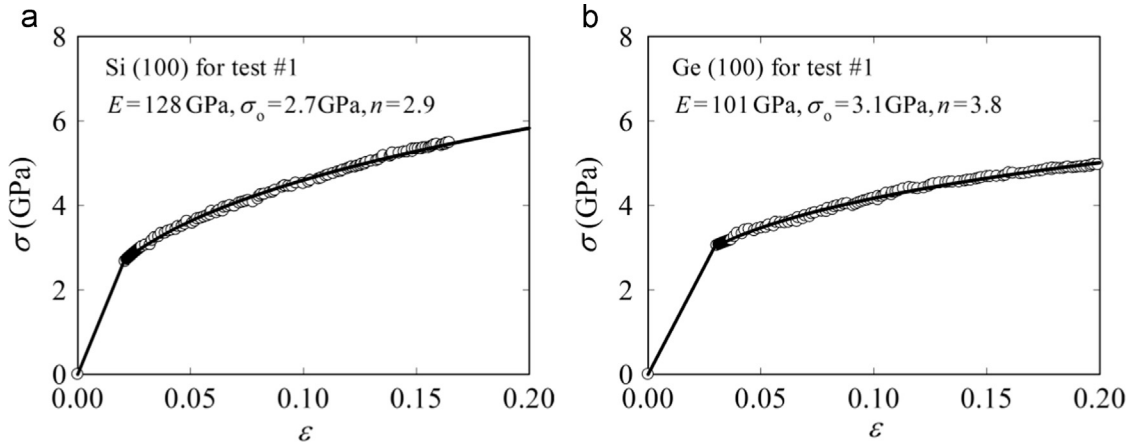

Fig. 14. Stress–strain curves for (a) Si (100) and (b) Ge (100).

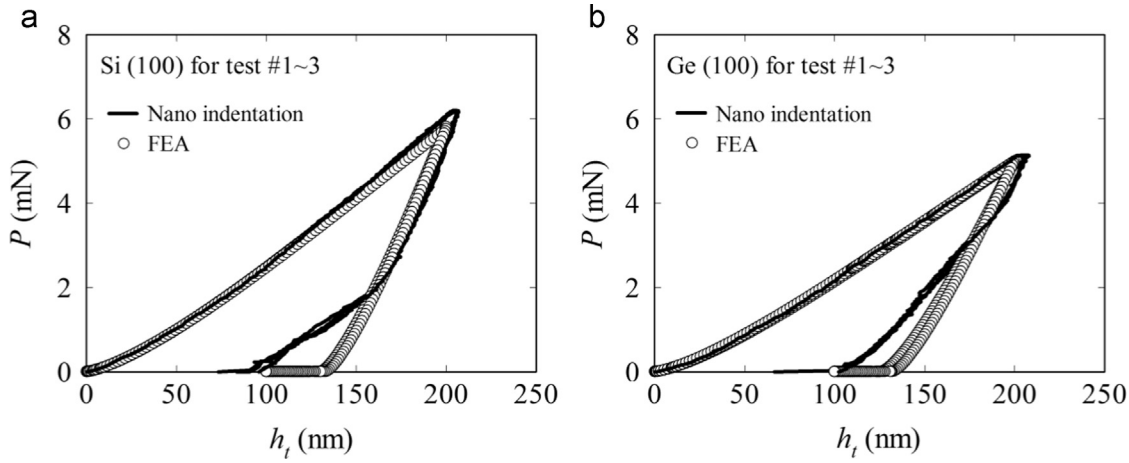

Fig. 15. Comparison of measured load–depth curves to those obtained from FEA. for Si (100) and Ge (100).

Acknowledgment

This research was supported by Basic Science Research Program through the National Research Foundation of Korea (No. NRF-2012 R1A2A2A 01046480).

References

[1] ASTM E8/E8M-13a. Standard test methods for tension testing of metallic materials. West Conshohocken, PA, USA: ASTM International; 2013.
[2] Cheng YT, Cheng CM. Scaling approach to conical indentation in elasto-plastic solids with work hardening. J Appl Phys 1998;84:1284–91.
[3] Dao M, Chollacoop N, Van Vliet KJ, Venkatesh TA, Suresh S. Computational modeling of the forward and reverse problems in instrumented sharp indentation. Acta Mater 2001;49:3899–918.
[4] Giannakopoulos AE, Suresh S. Determination of elastoplastic properties by instrumented sharp indentation. Scr Mater 1999;40:1191–8.
[5] Hyun HC, Kim M, Lee JH, Lee H. A dual conical indentation technique based on FEA solutions for property evaluation. Mech Mater 2011;43:313–31.
[6] Kim M, Lee JH, Rickhey F, Lee H. A dual triangular pyramidal indentation techniques for material property evaluation. J Mater Res 2015;30:1098–109.
[7] Larsson P-L, Giannakopoulos AE, Soderlund E, Rowcliffe DJ, Vestergaard R. Analysis of Berkovich indentation. Int J Solid Struct 1996;33:221–48.
[8] Lee H, Lee JH, Pharr GM. A numerical approach to spherical indentation techniques for material property evaluation. J Mech Phys Solids 2005;53:2037–69.
[9] Lee H, Lee JH. Evaluation of material characteristics by micro/nano indentation tests. Trans KSME 2008;32:805–16.
[10] Lee JH, Kim T, Lee H. A study on robust indentation techniques to evaluate elastic–plastic properties of metals. Int J Solid Struct 2010;47:647–64.
[11] Tabor D. The hardness of metals. London: Oxford University Press; 1951.
[12] Beghini M, Bertini L, Fontanari V. Evaluation of the stress–strain curve of metallic metarials by spherical indentation. Int J Solid Struct 2006;43:2441–59.
[13] Cao YP, Lu J. A new method to extract the plastic properties of metal materials from an instrumented spherical indentation loading curve. Acta Mater 2004;52:4023–32.
[14] Field JS, Swain MV. Determining the mechanical properties of small volumes of material from submicrometer spherical indentation. J Mater Res 1995;10:101–12.
[15] Kang S-K, Kim Y-C, Kim K-H, Kim J-Y, Kwon D. Extended expanding cavity model for measurement of flow properties using insrtumented spherical indentation. Int J Plast 2013;49:1–15.
[16] Kucharski S, Mroz Z. Identification of yield stress and plastic hardening parameters from a spherical indentation test. Int J Mech Sci 2007;49:1238–50.
[17] Le M-Q. Material characterrization by instrumented spherical indentation. Mech Mater 2012;46:42–56.
[18] Nayebi A, El Abdi R, Bartier O, Mauvoisin G. A new method to extract the plastic properties of metal materials from an instrumented spherical indentation loading curve. Mech Mater 2002;34:243–54.
[19] Song Z, Komvopoulos K. Elastic–plastic spherical indentation: deformation regimes, evolution of plasticity, and hardening effect. Mech Mater 2013;61:91–100.
[20] Taljat B, Zacharia T, Kosel F. New analytical procedure to determine stress–strain curve from spherical indentation data. Int J Solid Struct 1998;35:4411–26.
[21] Yonez A, Akimoto H, Fujisawa S, Chen X. Spherical indentation method for measuring local mechanical properties of welded stainless steel at high temperature. Mater Des 2013;52:812–20.
[22] Albayrak IC, Basu S, Sakulich A, Yeheskel O, Barsoum MW. Elastic and mechanical properties of polycrystaline transparent Yttria as determined by indentation techniquies. J Am Ceram Soc 2010;93:2028–34.
[23] Abaqus Version 6.12 User's manual. Dassault Systems Simulia Corp: Providence. RI, USA; 2012.
[24] Vander Voort GF. Metallography principles and practice. OH, USA: ASM international; 1984.
[25] Rice JR, Rosengren GF. Plane strain deformation near a crack-tip in a power law hardening material. J Mech Phys Solids 1968;16:1–12.
[26] Hay J, Crawford B. Measuring substrate-independent modulus of thin films. J Mater Res 2011;26:727–38.
[27] Sneddon IN. The relation between load and penetration in the axisymmetric Boussinesq problem for a punch of arbitrary profile. Int J Eng Sci 1965;3:47–57.
[28] Pharr GM, Oliver WC, Brotzen FR. On the generality of the relationship among contact stiffness, contact area and elastic modulus during indentation. J Mater Res 1992;7:613–7.
[29] Hill R, Storakers B, Zdunek AB. A theoretical study of the Brinell hardness test. Proc R Soc Lond Ser A 1989;423:301–30.
[30] Rickhey F, Lee JH, Lee H. An efficient way of extracting creep properties from short-time spherical indentation tests. J Mater Res 2015;30:3542–52.
[31] Ma Z, Long S, Pan Y, Zhou Y. Creep behavior and its influence on the mechanics of electrodeposited nickel films. J Mater Sci Technol 2009;25:90–4.
[32] Feng G, Ngan AHW. Effects of creep and thermal drift on modulus measurement using depth-sensing indentation. J Mater Res 2002;17:660–8.
[33] Tang B, Ngan AHW. Accurate measurement of tip–sample contact size during nanoindentation of viscoelastic materials. J Mater Res 2003;18:1141–8.
[34] Wortman JJ, Evans RA. Young's modulus, shear modulus, Poisson's ratio in silicon and germanium. J Appl Phys 1965;36:153–6.
[35] Callister WD, Rethwisch DG. Material science and engineering: an introduction. USA: John Wiley & Sons, Inc; 2009.
[36] Brady JE, Williams JS, Wong-Leung J, Swain MV, Munroe P. Transmission electron microscopy observation of deformation microstructure under spherical indentation in silicon. Appl Phys Lett 2000;77:3749–51.